Numerical Prediction of Steady and Unsteady Performances of Contrarotating Propellers

Chang-Sup Lee, * Young-Gi Kim, † Myung-Chul Baek, ‡ and Jae-Hoon Yoo‡

Abstract

This paper describes the procedure to predict steady and unsteady performances of a contrarotating propeller(CRP) by a mixed formulation of the boundary value problem(BVP) for the flow around a CRP. The blade BVP is treated by a classical vortex lattice method, whereas the hub BVP is solved by a potential-based panel method. Blades and trailing wakes are represented by a vortex and/or source lattice system, and hubs are represented by normal dipole and source distributions.

Both forward and aft propellers are solved simultaneously, thus treating the interaction effect without iteration. The unsteady performance is computed directly in time domain. The new numerical procedure requires a large amount of storage and computing time, which is however no longer a limit in a modern computer system.

Sample computations show that the steady performance compares very well with the experiments. The predicted unsteady behavior shows that the dominant harmonics of the total forces are multiples of not only the number of blades of the forward and aft propellers but also the product of both blade numbers. The magnitude of the latter harmonics, present also in uniform oncoming flow, may reach about 50% of the mean torque for the aft propeller, which in turn may cause a serious vibration problem in the complicated contrarotating shafting system.

1 Introduction

With successful installations of CRP's to prototype ships in Japan[1][2], an ability to design CRP is now emerging again as a core subject among marine propulsor hydrodynamics. The successful fitting of the CRP system to merchant ships was only possible through the realization of the complicated coaxial counterrotating shaft and reliable gearing system.

The hydrodynamic design method for CRP is relatively well established for the case of traditional application to torpedo propulsion[3], whereas a new application to a full size vessel raises a need for reconsideration of the whole design process from the model

*Member, Chungnam National University
†Member, Chungnam National University; presently at R & D Center, Samsung Heavy Industries
‡Member, Samsung Heavy Industries

testing to the full-scale performance prediction. The CRP when installed behind a ship will suffer a more severe inflow variation than in torpedo with an axisymmetric wake, and hence it should be designed with more emphasis and care on the cavitation and unsteady performance.

The lifting surface theory with a good reputation in predicting the performance of a conventional single screw propulsor(see, for example, Kerwin and Lee[4]) may also be adopted in predicting the performance of the CRP. A good review of the design method of the CRP may be found in Cox and Reed[5], where they summarized the fundamental physics and important features of the CRP design and analysis and reviewed the development of the design method from the lifting line theory to the lifting surface method. Most recent design method considers the influence of the hub which is no longer a negligible size due to the coaxial shafting arrangement[6].

The CRP differs from the conventional single screw propellers most significantly in hydrodynamic interaction between the forward and aft propellers. For an accurate prediction of the performance it is therefore essential to treat the interaction terms more accurately. Most of the existing theories deals with the interaction of the two propellers in an average sense; that is, the induction of one propeller upon the other propeller location is averaged in the circumferential direction. Moreover the boundary value problem of each propeller is solved separately, assuming the influence of the other blades is known. It is therefore necessary to resort to an iterative procedure.

The forward propeller is influenced by the induced velocity of the aft propeller firstly through the downwash effect upon the blade surface and secondly through the deformation of the trailing vortex sheet. The change of the average pitch of the helical vortex will alter the loading condition of the forward propeller. The analysis of the aft propeller is even worse, since the propeller operates cutting through the singular vortex sheet trailing and rotating together with the forward propeller. The blades will therefore experience a severe inflow variation. Precise measurement of the flow field around the CRP is therefore vital in developing an analysis method for the CRP.

In the present paper, we deal with the contrarotating propeller by a mixed formulation of the boundary-value problem to describe the flow around the CRP. The blade BVP is treated by the vortex lattice method of Kerwin and Lee[4], where the strengths of the vortices are determined by satisfying the zero normal flux condition on the camber surface. The hub BVP, whose unknown is the normal dipole strength itself, is however solved by the potential-based panel method of Morino[7]. Unlike the traditional iterative solution method, the unknown vortices and normal dipoles of both propellers and hubs are determined simultaneously without iteration. Although the size of the matrix becomes very large, the elimination of updating of induced velocities on the other propeller ensures an improved convergence.

The behavior of the CRP is unsteady even in an open water condition, and hence in principle the interaction has to be treated in time domain. For the prediction of the steady performance, the field-point inductions computed by rotating the blades are averaged in the circumferential direction, but the real induced velocities are considered for the prediction of the unsteady characteristics.

2 Statement of Boundary Value Problem

Let us consider a set of contrarotating propellers operating in a nonuniform effective ship wake field. The fluid is assumed to be inviscid, irrotational and incompressible. Conservation of mass to the fluid volume V enclosed by the blade and hub surfaces and their trailing vortex sheets leads to the governing equation for the perturbation velocity potential ϕ as:

$$\nabla^2\phi(p) = 0, \quad p(\vec{x}) \in V \tag{1}$$

where $p(\vec{x})$ denotes a field point in V.

Motion of the fluid satisfying the Laplace equation (1) can be uniquely defined by imposing the following boundary conditions on the boundary surfaces, that is,

1. Quiescence condition at infinity S_∞:

$$\nabla\phi \to 0, \quad p(\vec{x}) \in S_\infty \tag{2}$$

2. Kinematic boundary condition on the blade and hub surfaces $S_{B\cup H}$:

$$\hat{n} \cdot \vec{U}_\infty + \frac{\partial\phi}{\partial n} = 0, \quad p(\vec{x}) \in S_{B\cup H} \tag{3}$$

where $\vec{U}_\infty$ is the oncoming velocity to the propeller.

3. Kutta condition at the trailing edge:

$$|(\nabla\phi)_{T.E.}| < \infty \tag{4}$$

4. Kinematic and dynamic boundary conditions on the wake surface S_W:

$$\Delta\frac{\partial\phi}{\partial n} = (\hat{n} \cdot \nabla\phi)^+ - (\hat{n} \cdot \nabla\phi)^- = 0 \tag{5}$$

$$\Delta p = p^+ - p^- = 0 \tag{6}$$

where p denotes the pressure, and + and - denote the upper and lower surface of the wake, respectively.

3 Integral Equations

From Green's theorem, we may first derive an expression for the perturbation potential in the flow field by distributing normal dipoles and sources on the solid surfaces, and normal dipoles on the shed vortex sheet.

The perturbation velocity potential in the fluid region may now be expressed as follows:

$$\begin{aligned}\phi(\vec{x}) = & \int_{S_{B\cup H}} \{-\phi(\vec{\xi})\}\frac{\partial}{\partial n_\xi}G(\vec{x};\vec{\xi})dS \\ & + \int_{S_{B\cup H}} \{\frac{\partial\phi}{\partial n}(\vec{\xi})\}G(\vec{x};\vec{\xi})dS + \int_{S_w} \{-\Delta\phi_w\}\frac{\partial}{\partial n_\xi}G(\vec{x};\vec{\xi})dS\end{aligned} \tag{7}$$

where $G(\vec{x};\vec{\xi})$ is the Green's function.

Due to the characteristics of singularities, the governing equation (1), and the quiescence condition (2), will automatically be satisfied.

We know the strength of the sources distributed on blade and hub surfaces from (3) and the strengths of shed dipoles on the trailing vortex sheet in terms of the dipole strength on blades or hubs by satisfying Kelvin's conservation of circulation. We now note that (7) becomes an integral equation for the unknown strength of normal dipoles on blade and hub surfaces. Here the potential function is the only unknown in the integral equation. This potential-based formulation, suggested by Morino[7], has been successfully applied to marine propellers by Lee, J.-T.[8], Hoshino[9] among others.

We may apply (7) in principle to the solution of the CRP, but expect a computational limit due to the requirement of large computer memory, at least in the case of unsteady problem. We therefore linearize the equation assuming that the blade thickness is small compared to the chordlength, and obtain the following:

$$\begin{aligned}\frac{\partial\phi}{\partial n_p} = \quad & \int_{S_B} \hat{n}\cdot\vec{\gamma}\times\nabla_p G dS + \int_{S_B}\sigma\frac{\partial G}{\partial n_p}dS \\ & + \int_{S_W}(\Delta\phi_w)\frac{\partial}{\partial n_p}\left(\frac{\partial G}{\partial n_w}\right)dS + \left(\frac{\partial\phi}{\partial n_p}\right)_{\text{hub}} \end{aligned} \tag{8}$$

where normal dipoles are replaced by the vorticity γ distributed on the camber surface of the propeller blade and the last term denotes the induced velocity due to singularities on the hub.

The above equation (8) is well-known lifting-surface formulation, which has been applied successfully in design and analysis of a single screw propeller. We will apply the velocity form of the integral equation (8) on the blade camber surface of both forward and aft propellers, and the potential-based formulation (7) to hub surfaces.

4 Discretization of Solid Surfaces

4.1 Blade Surface

For numerical computation, the continuous distribution of the vorticity is replaced by a discrete vortex lattice as in Kerwin and Lee[4]. Continuous sources representing the blade thickness effect are also replaced by line source segments, whose strengths are determined in a similar manner as in thin wing theory. As shown in Figure 1, the blade is discretized into M_p strips from the hub radius r_H to the tip radius R in the spanwise direction, and N_p panels in the chordwise direction. As in Kerwin and Lee, a uniform discretization spacing is adopted here in both directions with $M_p = 10$ and $N_p = 10$.

4.2 Hub Surface

The size of the hub for a CRP is relatively larger than that of a single screw propeller, and therefore the image effect of the hub surface has to be considered. The true shape of the

hub is however not so essential, and hence fore and aft portions of the hub are replaced by ellipsoids for which the minor axes are taken to be the same as the hub radius r_H and the major axes are assumed to be several chordlengths. Along the intersection of the blade and the hub, the streamwise discretization is forced to match the discrete vortex boundary on the blades. The trailing vortex at the hub of the aft propeller is modeled to follow the hub surface until the radius reaches $r/R = 0.1$, and then is separated from the hub maintaining the same radius downstream. The geometry of the discretized hub surface is also shown in Figure 1.

5 Modeling of Trailing Wake

Due to the action of the propeller, the axial velocity within the slipstream tube is increased and the radius of the tube is contracted. The exact location of the trailing vortex sheet should in principle be determined by satisfying the kinematic and dynamic boundary conditions on the wake surface as a part of the solution. Instead of solving the exact trailing vortex geometry, we will however adopt the model of Greeley and Kerwin[10] which has been successfully applied to the single screw propeller.

The geometry of the wake trailing each propeller of the CRP gives influence on the performance of each propeller as in the single screw propeller. Due to fore and aft coaxial arrangement of the CRP, the trailing wake of the forward propeller is however exposed to the direct influence of the aft propeller, which cuts through the vortex sheets of the forward propeller and hence at the same time meets the rapidly varying oncoming flow. In the present paper, we assume that the shedding vortices emanate from the blade trailing edge following the mean helical lines whose pitch angles are determined by using the induced velocities and ship inflow.

The velocity diagram of the CRP is shown in Figure 2, where u_a and u_t denote the axial and tangential induced velocities, respectively. The subscript 1 or 2 denote the forward or aft propeller, respectively, and thus $(u_a)_{ij}$ implies the axial velocity at the i-th propeller induced by the j-th propeller. We may therefore express the total induced velocities as follows:

$$\begin{aligned} (u_a)_i &= (u_a)_{ii} + (u_a)_{ij} \\ (u_t)_i &= (u_t)_{ii} + (u_t)_{ij} \end{aligned} \tag{9}$$

for i, $j = 1, 2$. We observe that $(u_t)_{12}$ is zero and $(u_a)_{12}$ is also very small.

The induced velocities are averaged in the circumferential direction, thus forming the helical shape with a hydrodynamic pitch angle as may be seen in Figure 2. Deviation of the geometry from the average in the unsteady case is assumed negligible. Figure 3 shows the typical wake patterns of the CRP. Note that the two wake surfaces intersect each other.

6 Numerical Procedure

6.1 Calculation of Induced Velocity and Potential

The induced velocity due to the vortex system is calculated by applying the famous law of Biot-Savart. For details on induced velocities by the discrete vortex and source segments, see Kerwin and Lee[4]. Induced potentials due to the normal dipoles and sources distributed on the hyperboloidal surface panel may be computed by formulae suggested by Morino[7].

For an accurate analysis of the CRP, the interaction of the forward and aft propellers has to be evaluated carefully. Since the numbers of the blades of both propellers are finite, the induced velocity varies with time and position.

The induced velocity or potential upon the control points on the aft blades due to the wake vortex sheet of the forward blades has to be computed with a special care, since the aft blades cut through the vortex wake trailing the forward propeller. To avoid a possible singular behavior in computing the induction, we first look for the nearest point, that is the geometric center on the trailing wake vortex panel, from the control point on the aft blade by comparing the axial and radial coordinates of both points, and then we relocate the control point on the corresponding point on the forward trailing wake panel. The induced velocity is then computed on the newly obtained control points, which will be rotated between two adjacent wake sheets of the forward propeller to get the time history of the induction.

For the prediction of the unsteady behavior, it is necessary to keep in storage the time-varying quantities such as the inductions as a function of relative angular position of both propellers, requiring a large memory size.

When we have interests only in the mean thrust and torque of the CRP, the mutual interaction of both propellers may be assumed to be independent of time. The induced velocities in such case are computed at the field points whose angular positions are selected satisfying the rule of Gaussian quadrature, and can be averaged in the circumferential direction.

6.2 Solution Procedure

The solution procedure for the unsteady performance is basically the same as the time-marching iterative method of Kerwin and Lee[4]. The boundary conditions on the camber surface are satisfied on a set of selected control points which are located at the geometric center of each rectangular vortex lattice on the blade. The boundary conditions on the hub surface are satisfied on the geometric center of each quadrilateral panel. Since the boundary value problems on both the propeller blades and the hub surfaces are solved at the same time, the size of the matrix is very large, but it is no longer necessary to resort to the iterative procedure solving the BVP of each propeller by turns.

Once the strengths of the vortices or the normal dipoles, the velocities on the field points and on the propeller blades are computed, and subsequently the pressures and forces are obtained as a function of discrete time steps.

7 Numerical Analysis and Results

To validate the present formulation and numerical procedure, we select two different sets of CRP; one is SSPA series CRP for commercial vessels and the other is DTRC CRP for high speed propulsion.

7.1 Test Propellers

SSPA K118 CR-Series: The SSPA CRP Series, designed by Bjarne[11], consists of 4 sets of CRP's and has the total thrust coefficient $K_T = T/\rho n^2 D^4 = 0.38$. The number of blades and the expanded area ratio of the forward propeller are $Z_f = 4$ and $A_E = 0.4$, and the corresponding values for the aft propeller are $Z_a = 5$ and $A_E = 0.5$. Both propellers have the NACA a=0.8 mean camber line and NACA 16 thickness form. The pitch ratio varies from $P/D = 0.8$ to $P/D = 1.4$ to cover various ship types from the low speed tanker to the high speed container ship. For the present sample calculation, we select $P_{0.75}/D_f = 1.1$, the diameter ratio $D_a/D_f = 0.936$ and the gap between the propeller $a/D_f = 0.191$. Detail geometric data including the offsets may be found in [11].

DTRC CRP: The DTRC CRP 5067 and 5068(see Chen and Reed[6]) are designed for general high speed vessel. The forward propeller DTRC 5067 is designed to have $D_f = 6.1m$ and to rotate with $rpm_f = 51$. The aft propeller rotates with the same rpm as the forward propeller, but has smaller diameter ratio $D_a/D_f = 0.85$ so that the aft propeller operates within the tip vortex tube of the forward propeller. The gap ratio is $a/D_f = 0.25$. The numbers of blades of both propeller are $Z_f = 7$ and $Z_a = 5$. The designed thrust coefficient $K_T = 0.5849$ when the torque ratio is $Q_a/Q_f = 1.07$. Detailed data including the offsets may be found in [6].

7.2 Steady Analysis

SSPA K118 CR-Series: For the SSPA CRP, a systematic study is carried to check the various features of the CRP and also of the computing scheme. Among others the effect of the hub is correctly represented by the hyperboloidal panels; that is, the loading of the blade is increased due to the image effect compared to the hubless case. The rotational components of induced velocities from both propellers are shown to cancel each other $0.691D_f$ downstream from the forward propeller. Figure 4 shows the computed open water characteristics together with the experimental values of SSPA[11]. Except the low advance coefficient region the correlation is fairly good.

DTRC CRP(DTRC 5067+5068): For the DTRC CRP with $P_{0.75}/D_f = 1.94$, another systematic study is carried out. The influence of the hub for $J_A = 1.584$ is shown in Figure 5, which clearly indicates that the loading increases with the hub included and that the effect is more pronounced for the aft propeller. Figures 6 and 7 show the axial and tangential induced velocities, respectively, at $x/D_f = 0.75$ downstream of the forward propeller. Figure 7 indicates that the rotational energy shed from each propeller cancel each other as the designer intended. The open water performance of the CRP is presented

in Figure 8 together with the experiments at DTRC[6]. The prediction correlates very well in K_T, but slightly underpredicts in K_Q.

7.3 Unsteady Analysis

The DTRC CRP is chosen as a test propeller for the unsteady analysis. Since the storage requirement increases considerably, we reduced the numbers of the blades to $Z_f = 3$ and $Z_a = 2$, and the numbers of panels to $M_p = 5$ and $N_p = 5$. The advance coefficients of both propellers are $J_f = 1.0$ and $J_a = 1.1765$. The angular time step of the forward propeller is taken to be $\delta\theta_f = 6^o$, and that of the aft one is $\delta\theta_a = \delta\theta_f \times (J_f/J_a)$. The existence of the hub is neglected, since the effect of the hub is secondary in unsteady problem.

The K_T variations on the key blades of both propellers in open water are shown in Figure9. Note that the forward propeller is influenced by the aft propeller slightly, but the aft propeller operating in the wake of the forward propeller experiences drastic change of angle of attack on the blade. Figure 10 shows the results of Fourier analysis where we notice that the harmonic of order $Z_f \times Z_a = 6$ is most pronounced, reaching to about 30% of the mean thrust(to about 50% for torque). This phenomenon is not observed for the single screw propeller. Have we selected the true numbers of blades, we may expect an exciting force of order $Z_f \times Z_a = 35$, which may cause a complete different kind of vibration problem to the vessel.

To see the influence of the ship wake, we arbitrarily selected a realistic wake of a high speed container ship and carried out extensive tests. Figure 11 shows the thrust variation in behind condition and compares with the open water case in Figure9. We observe the loading of the forward propeller is dependent more on the ship wake, however the loading characteristics of the aft propeller is still similar to that of the open water case. This result implies that the influence of the trailing wake of the forward propeller is more severe than the ship wake variation. The harmonic analysis supports this observation. Figure 12 concludes that the unsteady analysis of the CRP should be focused more on the harmonic component of the product of the numbers of blades of both propellers.

8 Conclusions

A numerical method to predict the steady and unsteady performances of the CRP is now established.

1. A hybrid method treating the blade BVP by the discrete vortex method and the hub by the surface panel method is formulated, and the whole BVP of the forward and aft propellers is solved simultaneously.

2. The interaction of both propellers is averaged to get the wake geometry, but is considered exactly in the unsteady analysis.

3. Sample computations with both the low speed SSPA CRP and the high speed DTRC CRP show good correlations with the experimental results, and hence the present method may be applicable to a practical design.

4. For the CRP, the unsteady forces are dominated by the interaction between the aft propeller and the shed wake trailing the forward propeller. The most significant harmonics are multiples of numbers of blades of both propellers.

5. An improvement in computational algorithm, especially in connection with the storage requirement, is needed for complete validation of the unsteady prediction.

References

[1] Nishiyama, S., Sakamoto, Y., Ishida, S., Fujino, R. and Oshima, M., "Development of contra-rotating propeller systems for Juno - A 37,000 DWT class bulk-carrier," *Trans. SNAME*, Vol. 98, 1990.

[2] Nakamura, S., Ohta, T., Yonekura, K, Sasajima, T. and Saki, K., "World's first contra-rotating propeller system successfully fitted to a merchant ship," 11th International Marine Propulsion Conference & Exhibition, March 9-10, 1989, 12 p.

[3] Morgan, W.B., "The design of contrarotating propellers using Lerbs' theory," *Trans. SNAME*, 1960, 26p.

[4] Kerwin, J. E. & Lee, C.-S., "Prediction of steady and unsteady marine propeller performance by numerical lifting surface theory," *Trans. SNAME*, Vol. 86, Soc. of Naval Arch. & Marine Eng., 1978, pp. 218-258

[5] Cox, B.D. and Reed, A.M., "Contrarotating propellers-Design theory and application," SNAME Propeller '88 Symposium, Virginia Beach, Sept. 20-21, 1988, 29p.

[6] Chen, B. Y.-H. and Reed, A.M., "A design method and an application for contrarotating propellers," DTRC R. & D. 90-003, 1990, 21p.

[7] Morino, L. and Kuo, C.-C., " Subsonic potential aerodynamic for complex configurations: a general theory," *AIAA Journal*, Vol. 12, No. 2, 1974, pp. 191-197.

[8] Lee, J.-T., "A potential-based panel method for the analysis of marine propellers in steady flow," Ph.D. Thesis, Department of Ocean Engineering, M.I.T., Cambridge, Mass., 1987.

[9] Hoshino, T., "Hydrodynamic analysis of propellers in steady flow using a surface panel method," *J. of Soc. of Naval Arch. of Japan*, Vol. 165, 1989, pp. 55-70.

[10] Greeley, D.S. & Kerwin, J.E., "Numerical methods for propeller design and analysis in steady flow," *Trans. SNAME*, Vol. 90, 1982.

[11] Bjarne, E., "Systematic studies of contra-rotating propellers for merchant ship," Proc. IMAS 73, 1973, pp. 49-59.

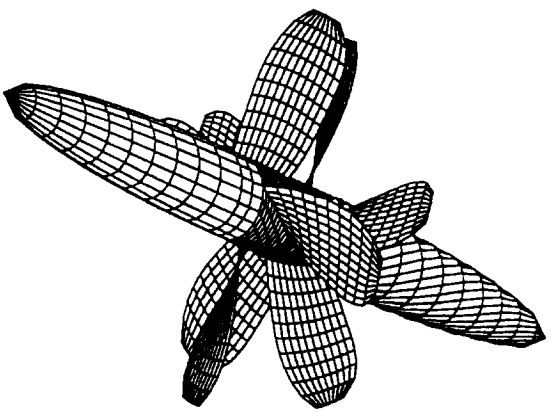

Figure 1: Perspective view of SSPA CRP

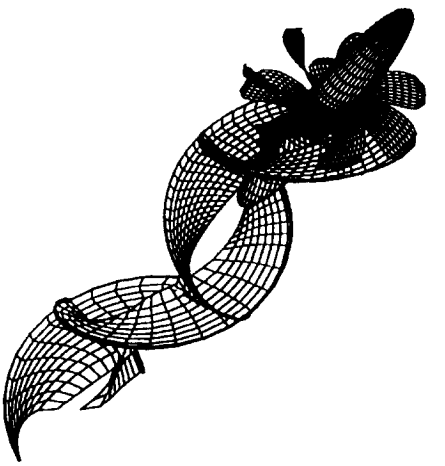

Figure 3: Perspective view of DTRC CRP with wake

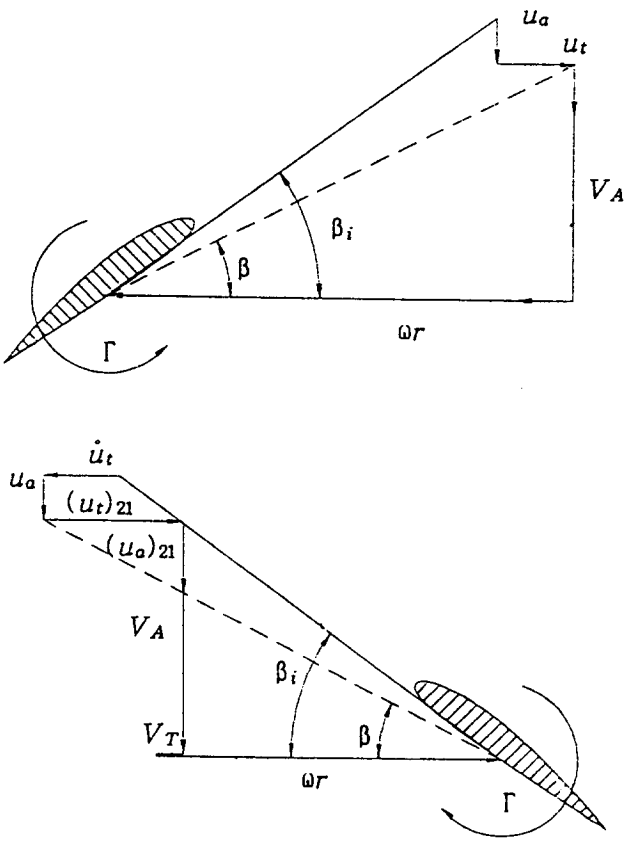

Figure 2: Relative velocities at blade sections

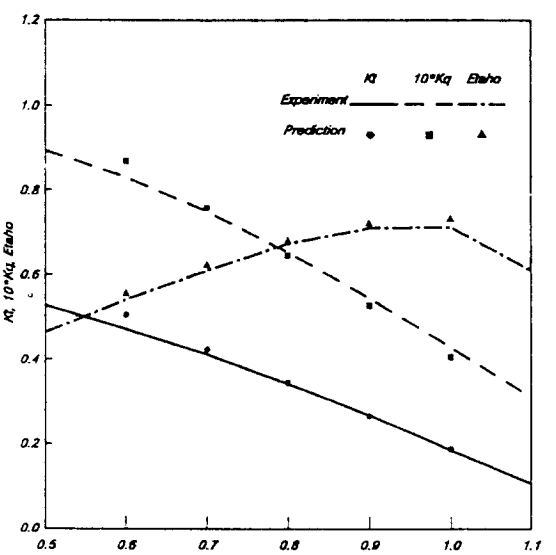

Figure 4: Open water characteristics of SSPA CRP with $P/D_f = 1.1$

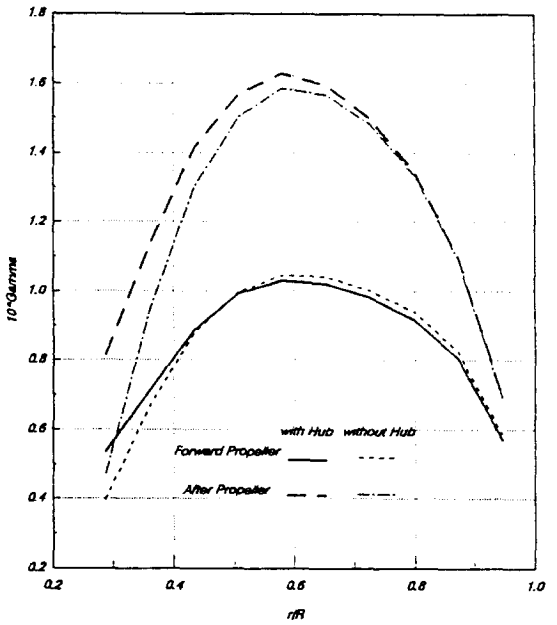

Figure 5: Circulation distribution on DTRC CRP

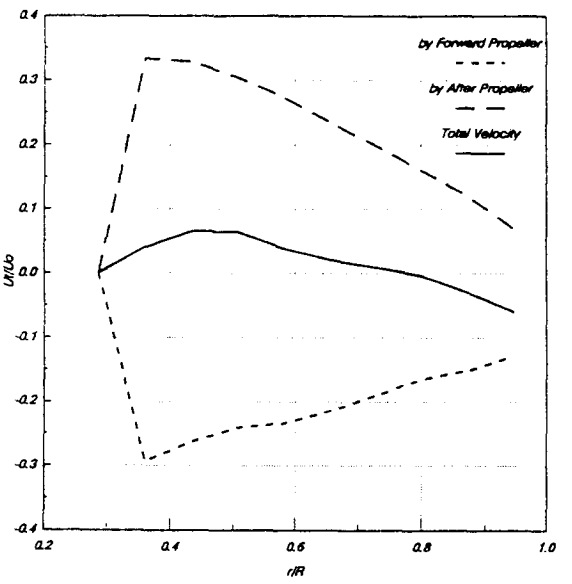

Figure 7: Radial distribution of tangential velocities for DTRC CRP at $x/D_f = 0.75$

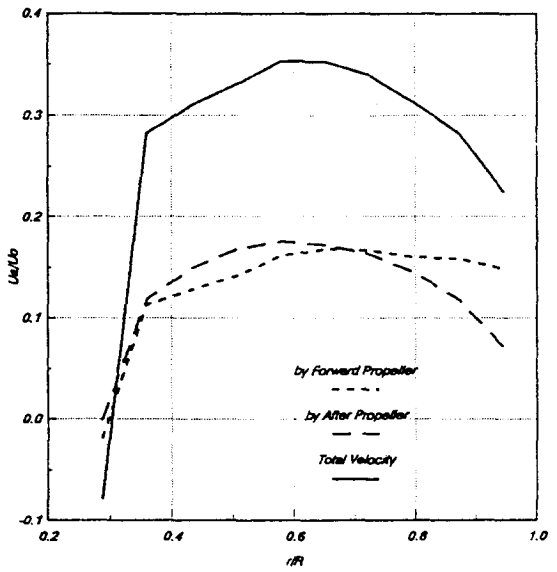

Figure 6: Radial distribution of axial induced velocities for DTRC CRP at $x/D_f = 0.75$

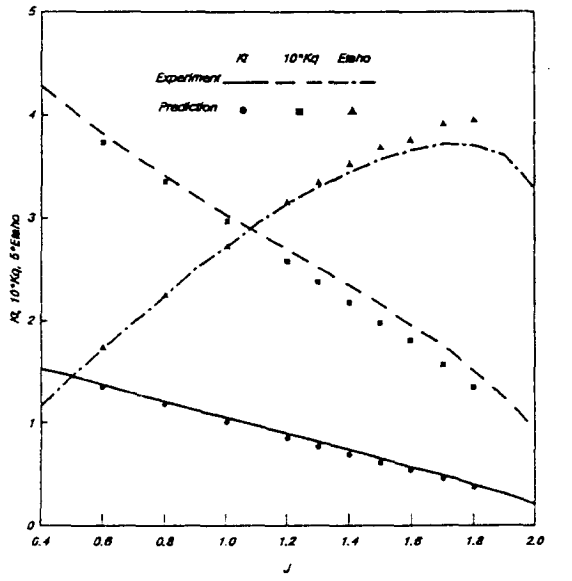

Figure 8: Open water characteristics of DTRC CRP

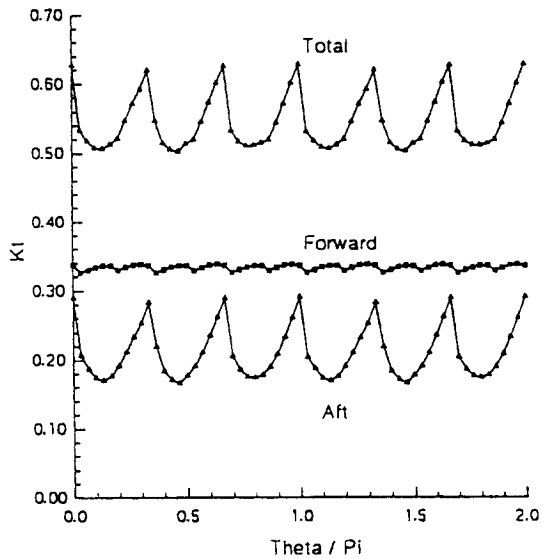

Figure 9: Thrust variation on DTRC CRP in uniform flow

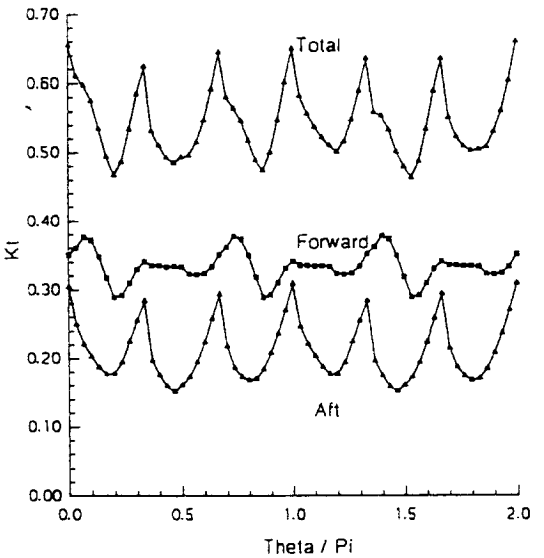

Figure 11: Thrust variation on DTRC CRP in ship wake

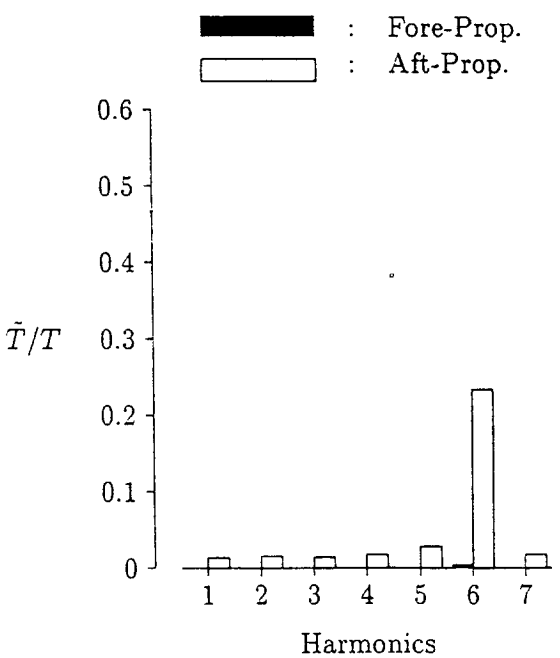

Figure 10: Harmonic components of thrust on DTRC CRP in uniform flow

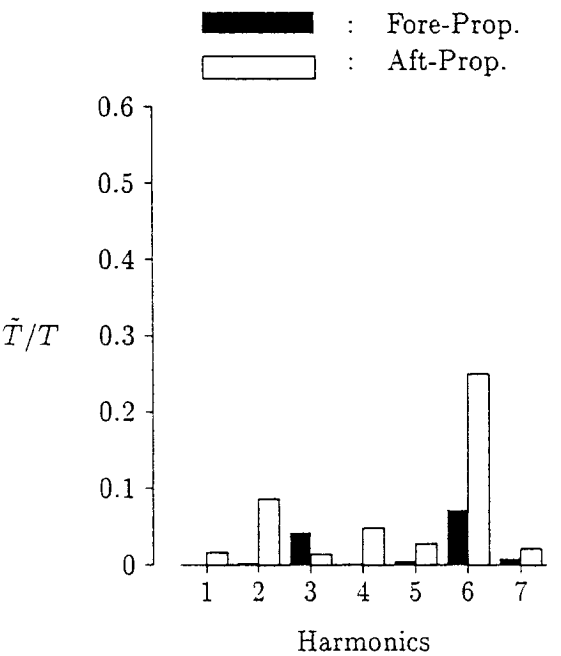

Figure 12: Harmonic components of thrust on DTRC CRP in ship wake